

REPORTS

42. Y. Amelin, E. Y. Ritsk, L. A. Neymark, *Earth Planet. Sci. Lett.* **148**, 299 (1997).
43. Individual chondrules were extracted from the Acfer 059 meteorite by using stainless-steel tools. Fractions consisting of chondrule fragments of uniform appearance were picked from a coarsely crushed portion of the meteorite. Chondrules and fragments were first cleaned by ultrasonic agitation in ethanol to remove adhering matrix minerals, weighed, and crushed to about <50 μm pieces with an aluminum oxide mortar and pestle. Preparation of the CAI fractions was similar, but the starting CAI fragments were coarsely crushed instead of pulverizing. Final cleaning was performed by five or six 10-min cycles of ultrasonic agitation in 0.5 to 2.0 M high-purity HCl in Savillex vials, which were subsequently used for digestion. During early analyses (chondrules 1 to 5), acid leachates from several fractions were preserved and analyzed separately. One chondrule and matrix sample were analyzed without acid leaching. During the later stages, chondrules were subjected to a more intensive acid leaching before crushing: three to five 30-min cycles of ultrasonic agitation in ethanol plus 6 M HCl 1:1 mixture. This treatment effectively removed all residual matrix from the surface of chondrules and helped to minimize the common Pb content, but it also caused etching and, in some cases, bleaching of chondrules and chondrule fragments. In addition, this treatment partially removed chondrule rims.
44. Y. Amelin, *Lunar Planet Sci.* **32**, 1389 (2001).
45. E. Rotenberg, Y. Amelin, *Eleventh Annual V.M. Goldschmidt Conference*, Hot Springs, VA, 20 to 24 May 2001, no. 3626.
46. Y. Amelin, in preparation.
47. J. W. Arden, G. Cressey, *Geochim. Cosmochim. Acta* **48**, 1899 (1984).
48. Primordial Pb is the Pb present in the solar system at the time of its formation. This is the least radiogenic Pb known, which is preserved, nearly unchanged, in the mineral troilite (FeS) in some iron meteorites (58, 59). Modern common Pb is a mixture of primordial Pb and 20 to 50% additions of radiogenic ^{206}Pb , ^{207}Pb , and ^{208}Pb accumulated since formation of the Earth and meteorite parent bodies.
49. F. Tera, R. W. Carlson, *Geochim. Cosmochim. Acta* **63**, 1877 (1999).
50. "Errorchron" is a term for an isochron with the scatter of the data exceeding analytical uncertainties. The excess scatter implies that the conditions of isochron model were not precisely fulfilled, e.g., the samples are not coeval, or the common Pb isotopic composition is variable, or the U-Pb systems of the samples were disturbed in the past. Thus, the errorchron dates may be inaccurate and should be interpreted with caution.
51. Y. Amelin *et al.*, *Lunar Planet Sci.* **33**, 1151 (2002).
52. J. H. Chen, G. J. Wasserburg, *Earth Planet. Sci. Lett.* **52**, 1 (1981).
53. Mg isotope compositions were measured with PAN-URGE, a modified Cameca IMS-3f ion microprobe, at Lawrence Livermore National Laboratory, with the operating conditions and procedures as described (60). The Mg isotope ratios were corrected for both instrumental and intrinsic fractionation, assuming the standard ratios of $^{25}\text{Mg}/^{24}\text{Mg} = 0.12663$ and $^{26}\text{Mg}/^{24}\text{Mg} = 0.13932$ (61). The corrected ratios ($^{26}\text{Mg}/^{24}\text{Mg}$)_c were used to calculate $\delta^{26}\text{Mg} = [(^{26}\text{Mg}/^{24}\text{Mg})_c / 0.13932 - 1] \times 1000$.
54. D. J. Cherniak, *Chem. Geol.* **177**, 381 (2001).
55. The error of 1.2 Myr in the CAI to chondrule formation interval (a simple sum of individual errors) is the most conservative estimate, which corresponds to the case of anticorrelated errors. A more probable estimate, for the case of uncorrelated errors, is 0.9 Myr (a quadratic sum of individual errors).
56. A. P. Boss, *Lunar Planet. Sci.* **31**, 1084 (2000).
57. G. Faure, *Principles of Isotope Geology* (Wiley, New York, 1986).
58. M. Tatsumoto, R. J. Knight, C. J. Allégre, *Science* **180**, 1279 (1973).
59. C. Göpel, G. Manhés, C. J. Allégre, *Geochim. Cosmochim. Acta* **49**, 1681 (1985).
60. I. D. Hutcheon, J. A. Armstrong, G. J. Wasserburg, *Geochim. Cosmochim. Acta* **51**, 3175 (1987).
61. E. J. Catanzaro, T. J. Murphy, E. L. Garner, W. R. Shields, *J. Res. Natl. Bur. Stand.* **70A**, 453 (1966).
62. We are grateful to A. Greshake for providing samples of Acfer 059. This work was supported by Canadian Space Agency contract 9F007-01012B/001/SR (Y.A., principal investigator) and NASA grants NAG5-10610 (A.N.K., principal investigator) and NAG5-11591 (K. Keil, principal investigator). Work performed under the auspices of the U.S. Department of Energy by Lawrence Livermore National Laboratory under contract W-7405-ENG-48.

Supporting Online Material

www.sciencemag.org/cgi/content/full/297/5587/1678/DC1

Table S1

14 May 2002; accepted 29 July 2002

Diamond Genesis, Seismic Structure, and Evolution of the Kaapvaal-Zimbabwe Craton

Steven B. Shirey,^{1*} Jeffrey W. Harris,² Stephen H. Richardson,³ Matthew J. Fouch,⁴ David E. James,¹ Pierre Cartigny,⁵ Peter Deines,⁶ Fanus Viljoen⁷

The lithospheric mantle beneath the Kaapvaal-Zimbabwe craton of southern Africa shows variations in seismic P-wave velocity at depths within the diamond stability field that correlate with differences in the composition of diamonds and their syngenetic inclusions. Middle Archean mantle depletion events initiated craton keel formation and early harzburgitic diamond formation. Late Archean accretionary events involving an oceanic lithosphere component stabilized the craton and contributed a younger Archean generation of eclogitic diamonds. Subsequent Proterozoic tectonic and magmatic events altered the composition of the continental lithosphere and added new lherzolitic and eclogitic diamonds to the Archean diamond suite.

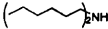
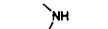
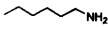
Seismic imaging of the lithospheric mantle beneath the Kaapvaal-Zimbabwe cratons and the Limpopo mobile belt (1-4) has produced a detailed picture of the source region for diamonds (Fig. 1). We place two decades of study of some 4000 diamonds from southern Africa's major diamond deposits (5, 6) into geologic context at lithospheric source depths to relate diamond formation to the processes

of craton creation, assembly, and modification. Diamond formation worldwide is associated with the presence of ancient lithospheric mantle keels beneath cratons (7, 8). In the Archean keel of the Kaapvaal-Zimbabwe craton, mantle peridotite and eclogite host multiple generations of both Archean and Proterozoic (9) diamonds (6, 10, 11) that have been sampled by later kim-

Table 1. Seismic velocity of the lithospheric mantle, diamond composition ($\delta^{13}\text{C}$, N, and type Ia), and inclusion paragenesis for southern African diamonds. Seismic velocities are for P-waves (in % deviation from a cratonic reference model) through a 50-km-radius cylinder of mantle extending from 150 km to 225 km depth below the major diamond mines (2, 3). Studies of C isotopes and N have been carried out on more than 900 individual diamonds enclosing silicate, oxide, and sulfide inclusions. Parageneses (P, peridotitic; E, eclogitic; W, websteritic) are listed in order of abundance; subordinate parageneses are in parentheses. Nitrogen concentration is the average of the total diamond population as measured by Fourier transform infrared spectroscopy (FTIR); De Beers Pool data is measured by mass spectrometry. Type Ia data are the % of diamonds in the studied population with aggregated nitrogen >20 ppm. Sources of data are as follows: De Beers Pool (22, 23), Finsch (25, 29), Jagersfontein (28), Jwaneng (23), Koffiefontein (28), Letlhakane (51), Orapa (24, 52), Premier (25, 29, 53), Roberts Victor (27), and Venetia (54).

Location	Seismic velocity	$\delta^{13}\text{C}$ (‰)	N (ppm)	Type Ia (%)	Paragenesis
Jwaneng	-0.006	-19 to -2	400	91	E,P
Letlhakane	-0.008		345	87	E,P
Orapa	-0.010	-26 to -3	478	94	E,P,(W)
Premier	-0.209	-14 to -2	413	90	E,P
Venetia	0.194	-18 to -2	259	77	P,(E,W)
De Beers Pool	0.245	-16 to -1	170	55	P,(E)
Finsch	0.084	-8 to -3	199	74	P,(E)
Roberts Victor	0.211	-16 to -3	260	73	P,(E)
Jagersfontein	0.357	-21 to -3	291	81	E,P
Koffiefontein	0.327	-17 to -2	201	85	P,E

Table 3. Hydroaminomethylation of different olefins. Reaction conditions: olefin, 15 mmol; amine, 15 mmol; [Rh(cod)₂]BF₄, 0.1 mol %; IPHOS, 0.4 mol %; toluene, 15 ml; THF, 15 ml; P_{CO}, 10 bar; P_{H₂}, 50 bar; temperature, 120°C; time, 24 hours.

Olefin	Amine	Conversion (%)	Total amine selectivity (%)	Linear amine selectivity (%)	lb	TON
		88	98	82	82:18	862
		71	69	53	72:28	490
		78	90	83	91:9	702
		100	65	74	78:22	650
		80	87	62	71:29	696
		77	91	76	78:22	701
		60	96	90	94:6	576
		88	96	68	71:29	563*

*3-Hexene, 10 mmol; piperidine, 10 mmol.

ing linear amines in good to excellent yields (Table 3). The reaction of 2-pentene and piperidine also proceeded smoothly in the presence of 0.05 mol % Rh [turnover number (TON) ≈ 2000]. However, a reaction time of 48 hours was needed to achieve complete conversion.

The reaction of the primary amine (*n*-hexylamine) occurs with high regio- and chemoselectivity, despite the further potential amination to yield tertiary amines. This reaction constitutes one of the rare examples of a hydroaminomethylation reaction of a primary amine to selectively give the secondary amine. In addition, 3-hexene, 3-octene, etc., also provide the corresponding linear amines preferentially under the present reaction conditions.

In general, the reaction sequences reported proceed with 90 to 95% atom efficiency and leave only water as the by-product. Although the catalyst productivity (TON = 2000) has already been developed to a useful level, further improvements should be possible.

References and Notes

1. A. Ricci, Ed., *Modern Amination Methods* (Wiley-VCH, Weinheim, Germany, 2000).
2. T. E. Müller, M. Beller, *Chem. Rev.* **98**, 675 (1998).
3. For a recent review, see (15).
4. L. A. van der Veen, P. C. J. Kamer, P. W. N. M. van Leeuwen, *Angew. Chem. Int. Ed.* **38**, 336 (1999).
5. D. Selent, K.-D. Wiese, D. Röttger, A. Börner, *Angew. Chem. Int. Ed.* **39**, 1639 (2000).
6. For a general review of hydroformylation of both internal and terminal olefins, as well as the ligand effects, see (16).
7. H. Klein, R. Jackstell, K.-D. Wiese, D. Röttger, M. Beller, *Angew. Chem. Int. Ed.* **40**, 3408 (2001).
8. For a general review of hydroaminomethylation reactions, see (17).
9. M. E. Broussard et al., *Science* **260**, 1784 (1993).
10. K. Tamao et al., *Tetrahedron Lett.* **16**, 1389 (1977).
11. W. A. Hermann, R. Schmid, C. W. Kohlpaintner, T. Priemeier, *Organometallics* **14**, 1961 (1995).

12. K. Weissermel, H.-J. Arpe, *Industrielle Organische Chemie* (Wiley-VCH, Weinheim, Germany, ed. 5, 2000).
13. P. W. N. M. van Leeuwen, P. C. Kamer, J. N. H. Reek, P. Dierkes, *Chem. Rev.* **100**, 2741 (2000).
14. All hydroaminomethylation experiments were carried

out in a Parr stainless steel autoclave (100 ml). In a typical experiment, the autoclave was charged with [Rh(cod)₂]BF₄ (0.1 mol %), IPHOS (0.4 mol %), piperidine (15 mmol), tetrahydrofuran (15 ml), and toluene (15 ml) under argon atmosphere. The autoclave was cooled with freezing mixture after closing, and 2-butene (15 to 16 mmol) was condensed into it. The autoclave was pressurized with CO (10 bar) and hydrogen (50 bar) and the reaction was carried out at 120°C for 24 hours. After reaction, the autoclave was cooled to 0° to 5°C and then depressurized, and the contents were transferred to a Schlenk flask under argon atmosphere, dried over MgSO₄, and analyzed by gas chromatography [HP-5890 series; column, HP5 (crosslinked 5% PH ME Siloxane), 30 m by 0.25 mm] using bis(methoxyethyl)ether as an internal standard.

15. M. Beller et al., *Synlett*, in press.
16. P. W. N. M. van Leeuwen, C. Claver, Eds., *Rhodium Catalyzed Hydroformylation* (Kluwer Academic, Dordrecht, Netherlands, 2000).
17. P. Eilbracht et al., *Chem. Rev.* **99**, 3329 (1999).
18. Additional examples are given in expanded tables at Science Online.
19. We thank A. Tillack for general discussions. Supported by a fellowship from the Alexander-von-Humboldt-Stiftung (A.S.) and by the state Mecklenburg-Vorpommern, Fonds der Chemischen Industrie, and Bundesministerium für Bildung und Forschung.

Supporting Online Material

www.sciencemag.org/cgi/content/full/297/5587/1676/DC1

Materials and Methods
Tables S1 and S2

7 June 2002; accepted 23 July 2002

Lead Isotopic Ages of Chondrules and Calcium-Aluminum-Rich Inclusions

Yuri Amelin,^{1*} Alexander N. Krot,² Ian D. Hutcheon,³ Alexander A. Ulyanov⁴

The lead-lead isochron age of chondrules in the CR chondrite Acfer 059 is 4564.7 ± 0.6 million years ago (Ma), whereas the lead isotopic age of calcium-aluminum-rich inclusions (CAIs) in the CV chondrite Efremovka is 4567.2 ± 0.6 Ma. This gives an interval of 2.5 ± 1.2 million years (My) between formation of the CV CAIs and the CR chondrules and indicates that CAI- and chondrule-forming events lasted for at least 1.3 My. This time interval is consistent with a 2- to 3-My age difference between CR CAIs and chondrules inferred from the differences in their initial ²⁶Al/²⁷Al ratios and supports the chronological significance of the ²⁶Al-²⁶Mg systematics.

Chondritic meteorites (chondrites) consist of three major components: refractory CAIs, less refractory ferromagnesian silicate spherules

called chondrules, and a fine-grained matrix. It is generally believed that CAIs and chondrules formed in the solar nebula (a disk of dust and gas surrounding the proto-Sun) by high-temperature processes that included condensation, evaporation, and, for all chondrules and many CAIs, subsequent melting during multiple brief heating episodes (1–3). The mechanisms involved in chondrule formation are uncertain: shock waves, lightning discharges, and X-wind (jet flow) are currently being considered (2, 4–8). The existing estimates for the timing of CAI and chondrule formation are either controversial or insufficiently precise. Thus, the total duration of CAI and chondrule formation,

¹Department of Earth Sciences, Royal Ontario Museum, Toronto, ON M5S 2C6, Canada. ²Hawaii Institute of Geophysics and Planetology, School of Ocean and Earth Science and Technology, University of Hawaii, Honolulu, HI 96822, USA. ³Lawrence Livermore National Laboratory, Livermore, CA 94451, USA. ⁴M. V. Lomonosov Moscow State University, Moscow 117999, Russia.

*Present address: Geological Survey of Canada, 601 Booth Street, Ottawa, ON K1A 0E8, Canada.

†To whom correspondence should be addressed. E-mail: yamelin@NRC.nrc.ca

REPORTS

which can provide important constraints on their origin, remains obscure.

CAIs and chondrules formed with different initial contents of the short-lived radionuclide ^{26}Al [half-life ($t_{1/2}$) ~ 0.73 Ma]. Most CAIs show large excesses of its decay product, $^{26}\text{Mg}^*$, corresponding to an initial $^{26}\text{Al}/^{27}\text{Al}$ ratio [$(^{26}\text{Al}/^{27}\text{Al})_i$] of $\sim 4 \times 10^{-5}$ to 5×10^{-5} (9). Chondrules, in contrast, show only small or undetectable $^{26}\text{Mg}^*$, implying $(^{26}\text{Al}/^{27}\text{Al})_i \leq 1.5 \times 10^{-5}$ (10–12). This difference may indicate that CAIs formed at least 1 to 2 My earlier than chondrules (9–13). This chronological interpretation is based on the assumption that ^{26}Al had a stellar origin (such as from a supernova, asymptotic giant branch star, or Wolf-Rayet star) and was injected and homogenized in the solar nebula over a time scale that was short compared to its half-life (14). A stellar origin for ^{26}Al is consistent with correlated abundances of ^{26}Al and ^{41}Ca ($t_{1/2} \sim 0.1$ Ma) in CAIs from the CV (Vigarano-like) and CM (Murchison-like) carbonaceous chondrites (15). However, the observed heterogeneity in ^{26}Al distribution among CAIs from the CH (ALH85085-like) carbonaceous chondrites (16), and the possibility that the ^{26}Al - ^{26}Mg systematics in chondrules and CAIs has been disturbed by late-stage asteroidal processing (17, 18), casts doubt on its chronological significance.

The alternative nonchronological interpretation of $^{26}\text{Al}/^{26}\text{Mg}$ systematics involves a local origin of ^{26}Al by energetic particle irradiation near the proto-Sun, resulting in radial heterogeneity of ^{26}Al distribution (4, 19). According to this interpretation, chondrules formed contemporaneously with CAIs, but farther away from the Sun (4). Although the detection in CAIs of the short-lived radionuclides ^{10}Be ($t_{1/2} \sim 1.5$ Ma) and ^7Be ($t_{1/2} \sim 52$ days), which can be produced only by nuclear spallation reactions (20, 21), may support the irradiation origin of ^{41}Ca and the short-lived radionuclide ^{53}Mn ($t_{1/2} \sim 3.7$ Ma), this mechanism still remains problematic for ^{26}Al (20, 22). The uncertainty of origin (stellar versus irradiation) of ^{53}Mn and ^{41}Ca hampers the chronological significance of the ^{53}Mn - ^{53}Cr and ^{41}Ca - ^{41}K systematics. The possible use of the ^{53}Mn - ^{53}Cr systematics for distinguishing formation ages of CAIs and chondrules is additionally complicated by the unknown distribution (homogeneous versus heterogeneous) of ^{53}Mn , the unknown initial $^{53}\text{Mn}/^{55}\text{Mn}$ ratio of the solar system, and possible mobilization of Mn during thermal metamorphism (23–25).

In contrast to the ^{26}Al - ^{26}Mg and ^{53}Mn - ^{53}Cr systematics, which can provide only relative ages, the $^{207}\text{Pb}/^{206}\text{Pb}$ chronometer can provide absolute formation ages of CAIs and chondrules (26). The errors of $^{207}\text{Pb}/^{206}\text{Pb}$ dates can be as low as 0.5 to 1.5 My; thus, the $^{207}\text{Pb}/^{206}\text{Pb}$ chronometer may be suitable for resolving a potential 2- to 3-My age difference between CAIs and chondrules. The current best model

Pb-Pb age of CAIs from the Allende CV chondrite of 4566 ± 2 Ma (27, 28) is not sufficiently precise, however. Here, we report more precise Pb-Pb internal isochron (29) ages for two CAIs from the CV chondrite Efremovka (E60 and E49) and a similarly precise Pb isotopic age for chondrules from the CR (Renazzo-like) carbonaceous chondrite Acfer 059. For the CAI E60, we also report the ^{26}Al - ^{26}Mg systematics.

CR chondrites are among the most primitive meteorites: They escaped thermal metamorphism and suffered only aqueous alteration at temperatures below 100° to 150°C (30–33). The degree of aqueous alteration varies among CR chondrites; e.g., Al Rais and Renazzo contain abundant phyllosilicates and carbonates in their CAIs, chondrules, and matrices, whereas chondrules and CAIs in other CR chondrites, including Acfer 059, are virtually phyllosilicate-free (32–36). The CR CAIs have uniformly ^{16}O -enriched compositions (35) and the canonical $(^{26}\text{Al}/^{27}\text{Al})_i$ ratio of 4×10^{-5} to 5×10^{-5} (16, 36), suggesting that they preserved their primary isotopic characteristics undisturbed.

The vast majority of chondrules in CR chondrites are large (~ 0.7 to 1 mm in apparent diameter), FeNi-metal-rich, sulfide-free, and volatile-poor. Chondrule olivine and pyroxenes are Cr_2O_3 -rich (0.5 to 1 weight %) and FeO-poor (Fa/Fs $_{1-2}$). FeNi metal has a large range in Ni contents (4 to 14 weight %) with a solar Co/Ni ratio (32, 33). Many chondrules are surrounded by silica-bearing igneous rims (37). On the basis of these characteristics, it has been inferred that CR chondrules were formed at high ambient nebular temperatures and escaped remelting at low ambient temperatures (33, 37). In contrast to the CAIs, chondrules from CR chondrites contain only small or undetectable $^{26}\text{Mg}^*$. Preliminary Al-Mg results for chondrules from CR and CV chondrites suggest the range of $(^{26}\text{Al}/^{27}\text{Al})_i$ from $\sim 1 \times 10^{-5}$ to $< 3 \times 10^{-6}$ (12).

The CV chondrites are a diverse group of meteorites that experienced various degrees of aqueous and/or Fe-alkali metasomatic alteration and mild ($< 500^\circ\text{C}$) thermal metamorphism (38). The Efremovka meteorite is one of the least altered and metamorphosed CV chondrites, which, however, experienced relatively strong shock metamorphism (39). Two Efremovka CAIs studied for Mg and Pb isotopes are a forsterite-bearing Type B inclusion E60 and a compact Type A inclusion E49. E60 is a spherical (~ 15 mm in apparent diameter) inclusion composed of Al-Ti-diopside (8 to 18 weight % Al_2O_3 , 0.4 to 3.3 weight % TiO_2), melilite (Äk_{22-86}), anorthite, Mg-spinel, and Ca-rich forsterite (40). E49 is an ellipsoidal (~ 3.2 mm by 4.5 mm) inclusion composed of melilite (Äk_{16-36}) and Mg-spinel. Both CAIs are surrounded by spinel-melilite-Al-diopside Wark-Lovering rims and contain very minor secondary nepheline.

Acid-washed and untreated Acfer 059 chondrules, as well as acid leachates, and the Acfer 059 matrix were analyzed for U and Pb concentrations and Pb isotopic compositions (41–43). The concentration ranges for U [2.5 to 35 parts per billion (ppb)] and Pb (6 to 44 ppb) in acid-washed chondrules (Table 1) are similar to previously reported values in ordinary chondrite chondrules (44–46). The range of measured $^{206}\text{Pb}/^{204}\text{Pb}$ ratios covers almost two orders of magnitude from 23.3 to 2198 (Table 1). The matrix contains > 700 ppb of Pb with rather unradiogenic Pb isotopic composition ($^{206}\text{Pb}/^{204}\text{Pb} = 11.09$), which is within the range of values for the Allende matrix (47). Contamination of chondrule material with matrix would severely reduce the radiogenic character of Pb and compromise the age determinations. The low $^{206}\text{Pb}/^{204}\text{Pb}$ ratios and elevated Pb concentrations in acid leachates of chondrules, together with highly radiogenic Pb and low Pb concentration in most washed chondrules, demonstrate the efficiency of the acid washing (Table 1).

Multiple fractions from the Efremovka CAIs E60 and E49 were analyzed with similar techniques. The concentration range of U (11 to 36 ppb) in the acid-washed fractions from the CAIs is the same as in the Acfer 059 chondrules (Table 1). The Pb concentrations (22 to 97 ppb) are slightly higher than in the chondrules. Acid-washed CAI fractions have consistently radiogenic Pb with measured $^{206}\text{Pb}/^{204}\text{Pb}$ ratios between 203 and 1263. Acid leachates contain elevated concentrations of common Pb, but only small amounts of U.

Model $^{207}\text{Pb}/^{206}\text{Pb}$ dates for the Acfer 059 chondrules are calculated by using primordial Pb (48). The dates generally increase for more radiogenic Pb isotopic compositions, approaching the value of ~ 4564 Ma (Table 1). The variation of the dates with the measured $^{206}\text{Pb}/^{204}\text{Pb}$ suggests that the common Pb isotopic composition in the chondrules differs from that of primordial Pb. Although the bias in the model dates, related to inaccurate assumption of initial common Pb, decreases with increasing $^{206}\text{Pb}/^{204}\text{Pb}$, this bias can be eliminated only by calculating isochron dates instead of model dates (49). Because of the possibility of partial dissolution and preferential leaching of U or Pb during intensive acid washing, we consider only Pb-Pb dates (table S1).

The Pb-Pb isochron and “errorchron” (50) dates (Table 2) show a decrease in the dispersion of the data, expressed by mean square weighted deviation (MSWD) values when analyses having high common Pb contents are removed. This demonstrates not only that the common Pb in the chondrules differs from the primordial Pb, but also that two or more components of common Pb (e.g., primordial Pb and modern terrestrial common Pb introduced by

R E P O R T S

weathering) are present, and that these components are unevenly distributed among the chondrules. In order to obtain a highly precise and

accurate date, we applied isochron regression to the data with the lowest common Pb content, for which the variations in the initial Pb isotopic

compositions are insignificant compared with the analytical errors. The six most radiogenic Pb isotope data points define an isochron with

Table 1. Pb isotope data and model dates.

No.*	Fraction†	Weight (g)	U (ppm)**	Pb (ppm)**	²⁰⁶ Pb/ ²⁰⁴ Pb††	²⁰⁷ Pb/ ²⁰⁶ Pb date (Ma)‡‡	2σ error (Ma)
<i>Acfer 059</i>							
1	Chondrule 10 W	0.00637	0.0180	0.0382	2198	4564.1	0.8
2	Chondrule 7 W	0.01275	0.0085	0.0211	1694	4564.0	0.7
3	Chondrule 6 W	0.00919	0.0064	0.0152	512.7	4562.5	1.0
4	Chondrule fragm W	0.00816	0.0057	0.0137	510.7	4562.3	0.8
5	Chondrule fragm W	0.00205	0.0131	0.0311	474.9	4561.9	1.5
6	Chondrule fragm W‡	0.00574	0.0063	0.0159	395.6	4561.0	0.9
7	Chondrule fragm W§	0.00301	0.0153	0.0371	389.0	4563.3	1.4
8	Chondrule 5 W	0.00376	0.0351	0.0327	383.2	4566.8	1.1
9	Chondrule 11 W	0.00470	0.0063	0.0148	381.0	4562.4	0.9
10	Chondrule 9 W	0.01200	0.0063	0.0059	228.0	4562.2	1.9
11	Chondrule fragm W	0.00452	0.0025	0.0063	203.5	4557.3	2.0
12	Chondrule 8 W	0.02000	0.0049	0.0081	192.9	4564.5	0.9
13	Chondrule fragm W	0.00503	0.0233	0.0376	169.0	4562.9	1.2
14	Chondrule 1 W	0.00495	0.0137	0.0130	100.1	4561.5	1.5
15	Chondrule 2 W	0.00177	0.0042	0.0097	75.04	4560.0	3.8
16	Chondrule 5 W	0.00097	0.0273	0.0249	71.14	4558.3	2.4
17	Chondrule 1 W	0.00338	0.0066	0.0100	59.95	4556.7	2.2
18	Chondrule fragm W	0.00144	0.0192	0.0439	48.35	4553.1	2.2
19	Chondrule fragm W	0.00354	0.0116	0.0283	46.21	4560.8	2.3
20	Chondrule 2 W	0.00387	0.0050	0.0309	23.30	4547.6	3.2
21	Chondrule 1¶	0.00569	0.0877	0.1344	19.21	4515.5	2.5
22	Acid leachate of chondrule 2 split 1 (fr.15)#	–	0.0059	0.1020	18.11	4497.0	3.2
23	Acid leachate of chondrule 1 split 1 (fr.14)#	–	0.1318	0.1953	15.97	4493.7	3.2
24	Acid leachate of chondrule 2 split 2 (fr.20)#	–	0.0171	0.1689	13.55	4480.6	5.6
25	Acid leachate of chondrule 1 split 2 (fr.17)#	–	0.2723	0.4278	13.23	4468.2	5.6
26	Matrix¶¶	0.00622	0.2255	0.7678	11.09	4531.4	9.9
<i>Efremovka CAI E49</i>							
27	Clear fragments	0.00337	0.0289	0.0970	1263.10	4567.0	0.8
28	Clear fines	0.00128	0.0269	0.0913	572.00	4566.3	0.9
29	Clear fines	0.00271	0.0184	0.0533	474.54	4567.4	1.0
30	Clear and white fragments	0.00366	0.0189	0.0497	448.75	4566.8	0.8
31	Fragments with yellow staining	0.00070	0.0340	0.0818	332.70	4566.3	1.2
32	Clear fragments with black inclusions	0.00125	0.0184	0.0637	203.11	4566.0	1.1
33	Acid leachate of fraction 30#	–	0.0100	0.4004	18.29	4477.5	23.4
<i>Efremovka CAI E60</i>							
34	Clear fines	0.00414	0.0251	0.0443	548.10	4567.6	0.7
35	Clear fines	0.00834	0.0276	0.0530	539.80	4567.9	0.7
36	Fines	0.00292	0.0285	0.0502	524.78	4567.9	0.8
37	Clear fragments	0.01127	0.0325	0.0577	447.63	4568.3	0.8
38	Rusty fragments and fines	0.00984	0.0287	0.0567	420.43	4568.5	0.9
39	Intergrown clear and black	0.00269	0.0111	0.0224	414.66	4567.2	0.8
40	Clear small fragments	0.01042	0.0315	0.0618	411.15	4568.2	0.8
41	Clear larger fragments	0.01359	0.0305	0.0607	401.00	4569.2	1.0
42	Fines with yellow staining	0.00407	0.0298	0.0532	389.70	4567.6	0.8
43	Coarse clear fragments	0.00717	0.0356	0.0639	348.98	4567.4	0.8
44	White fragments	0.00488	0.0331	0.0592	334.10	4569.0	0.9
45	White fragments	0.00414	0.0326	0.0624	270.90	4568.2	0.9
46	Acid leachate of fraction 44#	–	0.0140	0.9007	17.92	4510.0	2.8
47	Acid leachate of fraction 45#	–	0.0155	0.4998	17.60	4509.1	2.7

*Fractions arranged in the order of descending ²⁰⁶Pb/²⁰⁴Pb ratios. †Fraction descriptions: W, acid washed; fragm, chondrule fragments picked from crushed meteorite. ‡Chondrule fragments bleached by acid wash. §Green fragments (due to the presence of phyllosilicates). ||Chondrules 1, 2, and 5 were split after crushing, and two or more fractions were analyzed separately. ¶Fractions analyzed without acid washing. #Concentrations of U and Pb in acid leachates are calculated relative to the weights of fractions before leaching. **U and Pb concentrations are calculated to the total weights before washing. ††Measured ²⁰⁶Pb/²⁰⁴Pb ratio, no corrections applied. ‡‡Dates calculated from isotopic ratios corrected for blank, spike, fractionation and primordial common Pb (58).

REPORTS

an age of 4564.7 ± 0.6 Ma, MSWD = 0.5 (Table 2, Fig. 1). The "errorchrons" shown in Table 2 give dates that agree with this best date, but are less precise due to excess scatter, caused mainly by the common Pb isotopic variations.

The Pb-Pb isochrons for the Efremovka CAIs (Table 2, Fig. 1) show no excess scatter and give consistent dates of 4567.17 ± 0.70 Ma (MSWD = 0.88) for all six analyzed acid-washed fractions from the CAI E49, and 4567.4 ± 1.1 Ma (MSWD = 1.09) for all 12 fractions from the CAI E60. The weighted average of these two dates gives the best estimate for the timing of the CAI formation of 4567.2 ± 0.6 Ma. This age agrees, within error, with the previous Pb-Pb age determinations for the CAIs from the CV chondrite Allende (27, 28, 51, 52). However, the age of the Efremovka CAIs obtained here is much more precise and is clearly resolved from the age of the Acfer 059 chondrules.

The $^{27}\text{Al}/^{24}\text{Mg}$ ratios and Mg isotopic compositions of spinel, pyroxene, and anorthite from the CAI E60 (Table 3), determined by in situ ion microprobe analysis (53), define a line with the slope of $(4.63 \pm 0.44) \times 10^{-5}$ on the Al-Mg evolution diagram (Fig. 2), which is indistinguishable from the canonical ($^{26}\text{Al}/^{27}\text{Al}$)₁ value (9).

Before applying the Pb-Pb dates to constrain the interval of CAI and chondrule formation, we need to check whether these dates are primary ages, or if they were affected by secondary processes. The possibility that the Pb isotopic system was reset by diffusion during thermal metamorphism can be evaluated by using the Pb diffusion parameters (54) and the closure temperature estimates previously applied to equilibrated ordinary chondrites (46). The closure temperature calculations show that the diffusion of Pb in pyroxene (presumably the main carrier of U) at 150°C (the peak temperature reached during aqueous alteration of CR chondrites) is slow and can be ruled out as a cause of Pb isotopic resetting. Mineralogical and isotopic evidence for the pristine nature of the Acfer 059 chondrules (34) and CAIs (35, 36) suggests that resetting due to aqueous alteration is also very unlikely. The date of 4564.7 ± 0.6 Ma should therefore correspond to the timing of chondrule formation. The pristine mineralogy of the Efremovka CAIs E60 and E49 and $^{26}\text{Al}/^{26}\text{Mg}$ systematics of E60 suggest that the data of 4567.2 ± 0.6 Ma corresponds to the timing of CAI formation.

The data presented here have several implications. Small errors of chondrule Pb-Pb isochron regression and the lack of excess scatter among the most radiogenic data points suggest that the chondrules formed within the short interval, probably less than the isochron error limits of 1.2 My. The available $^{26}\text{Al}/^{26}\text{Mg}$ data for the chondrules from CR chondrites (12) are not sufficiently precise to verify this inference.

Table 2. Summary of Pb-Pb isochron regressions. Isochron and errorchron regressions show a decrease in the dispersion of the data, expressed by MSWD values, when analyses having high $^{206}\text{Pb}/^{204}\text{Pb}$ are removed. Regression for the washed chondrule data with $^{206}\text{Pb}/^{204}\text{Pb} > 300$ (line 5) shows relatively small residual scatter (MSWD = 2.9). For the data points with $^{206}\text{Pb}/^{204}\text{Pb} > 395$ (line 6), no residual scatter is observed (MSWD < 1). This data set provides sufficient spread in $^{206}\text{Pb}/^{204}\text{Pb}$ ratios for precisely constraining the slope and intersection of the isochron and yields the most precise age of 4564.7 ± 0.6 Ma. Further elimination of relatively less radiogenic points, e.g., to $^{206}\text{Pb}/^{204}\text{Pb} > 500$ (line 7), decreases scatter to an even lower value, but the uncertainty of the isochron slope and intercept increases because of the smaller spread in $^{206}\text{Pb}/^{204}\text{Pb}$. This illustrates a fundamental limitation of the isochron model—the controversial requirement of sufficient spread of data points while maintaining the uniformity of initial Pb composition.

No.	Data points included (fraction numbers from Table 1)	$(^{204}\text{Pb}/^{206}\text{Pb}) -$ $(^{207}\text{Pb}/^{206}\text{Pb})$ isochron date (Ma)	2 σ error (Ma)	MSWD
<i>Acfer 059</i>				
1	All data (1–26)	4562.8	3.3	51
2	All except matrix (1–25)	4564.0	1.9	19
3	All chondrule analyses (1–21)	4563.8	1.6	14
4	All acid-washed chondrules (1–20)	4563.1	1.3	9.3
5	Acid-washed chondrules with $^{206}\text{Pb}/^{204}\text{Pb} > 300$ (1–9)	4563.1	3.5	2.9
6	Acid-washed chondrules with $^{206}\text{Pb}/^{204}\text{Pb} > 395$ (1–6)	4564.7	0.6	0.51
7	Acid-washed chondrules with $^{206}\text{Pb}/^{204}\text{Pb} > 500$ (1–4)	4564.5	1.3	0.017
<i>Efremovka CAI E49</i>				
8	All data (27–33)	4568.4	0.9	2.5
9	All acid-washed fragments and fines (27–32)	4567.2	0.7	0.88
<i>Efremovka CAI E60</i>				
10	All data (34–47)	4569.2	0.4	1.7
11	All acid-washed fragments and fines (34–45)	4567.4	1.1	1.09

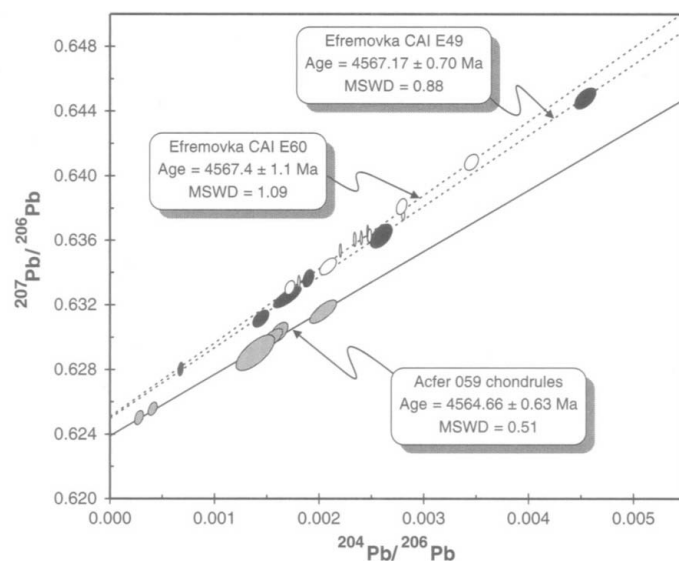


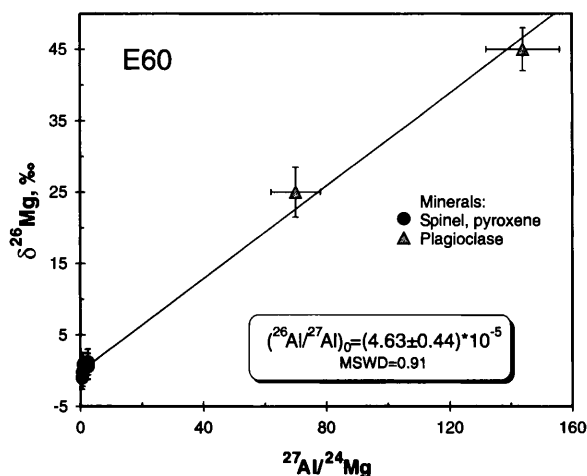
Fig. 1. Pb-Pb isochrons for the six most radiogenic Pb isotopic analyses of acid-washed chondrules from the CR chondrite Acfer 059 (solid line), and for acid-washed fractions from the Efremovka CAIs (dashed lines). $^{207}\text{Pb}/^{206}\text{Pb}$ ratios are not corrected for initial common Pb. Error ellipses are 2 σ . Isochron age errors are 95% confidence intervals.

Table 3. Al-Mg isotopic data for the CAI E60.

Mineral	$^{27}\text{Al}/^{24}\text{Mg}$	2 σ error	$\delta^{26}\text{Mg}$ (‰)*	2 σ error
Spinel 1	2.4	0.5	0.6	1.8
Spinel 2	2.4	0.5	1.2	1.8
Pyroxene 1	0.5	0.1	-1.0	1.6
Pyroxene 2	0.9	0.2	0.9	1.6
Pyroxene 3	0.6	0.1	-0.2	2.0
Plagioclase 1	70	8	25	3.5
Plagioclase 2	144	12	45	3.0

*Corrected for fractionation by normalizing to $^{25}\text{Mg}/^{24}\text{Mg} = 0.12663$. Per mil deviation relative to $^{26}\text{Mg}/^{24}\text{Mg} = 0.13932$ (67).

Fig. 2. Al-Mg evolution diagram for the Efremovka CAI E60. Error crosses are 2σ . Isochron initial $^{26}\text{Al}/^{27}\text{Al}$ error is a 95% confidence interval.



Combining the age of the Acfer 059 chondrules with the age of the CV CAIs gives an interval of 2.5 ± 1.2 My between formation of the CV CAIs and CR chondrules, which indicates that CAI- and chondrule-forming events in the solar nebula continued for at least 1.3 My (55). This time interval is consistent with a 2- to 3-My age difference between the CR CAIs and chondrules inferred from the reported differences in their $(^{26}\text{Al}/^{27}\text{Al})_i$ (12, 37). Together, these observations support the chronological significance of ^{26}Al - ^{26}Mg systematics (9) and are inconsistent with a local origin of ^{26}Al by energetic particle irradiation (19). The inferred 2- to 3-My age difference between CAIs and chondrules in CR chondrites (12, 36), which has yet to be confirmed by Pb-Pb dating of CAIs in CR chondrites, is inconsistent with the contemporaneous formation of CAIs and chondrules inferred in the X-wind model (4). The obtained estimate of the CAI-chondrule-formation interval of 2.5 ± 1.2 My is within the range of the X-wind (4), jet flow (5, 6), and shock-wave models (7, 8) of chondrule formation. However, the generation of strong chondrule-forming shocks for a period as long as 1 to 3 My could be a problem for the shock-wave model associated with the gravitational instability of the protoplanetary disk (8), which could have occurred only very early in the proto-Sun's evolution (56).

References and Notes

1. G. J. MacPherson, D. A. Wark, J. T. Armstrong, in *Meteorites and the Early Solar System*, J. F. Kerridge, M. S. Matthews, Eds. (Univ. of Arizona Press, Tucson, AZ, 1988), pp. 746–808.
2. A. E. Rubin, *Earth Sci. Rev.* **50**, 2 (2000).
3. A. J. Brearley et al., *Geochim. Cosmochim. Acta* **53**, 8 (1989).
4. F. H. Shu, S. Hsien, T. Lee, *Science* **271**, 1545 (1996).
5. K. Liffman, *Icarus* **100**, 608 (1992).
6. _____, A. Siora, *Mon. Not. R. Astron. Soc.* **290**, 629 (1997).
7. S. J. Weidenschilling, F. Marzari, L. L. Hood, *Science* **279**, 681 (1998).

8. S. J. Desch, H. C. Connolly Jr., *Meteorit. Planet. Sci.* **37**, 183 (2002).
9. G. J. MacPherson, A. M. Davis, E. K. Zinner, *Meteoritics* **30**, 365 (1995).
10. S. S. Russell, G. Srinivasan, G. R. Huss, G. J. Wasserburg, G. J. MacPherson, *Science* **273**, 257 (1996).
11. N. T. Kita, H. Nagahara, S. Togashi, Y. Morishita, *Geochim. Cosmochim. Acta* **64**, 3913 (2000).
12. K. K. Marhas, I. D. Hutcheon, A. N. Krot, J. N. Goswami, *Meteorit. Planet. Sci.* **35**, A102 (2000).
13. S. Mostefaoui et al., *Meteorit. Planet. Sci.* **37**, 421 (2002).
14. J. N. Goswami, H. A. T. Vanhala, in *Protostars and Planets IV*, M. Mannings, A. P. Boss, S. S. Russell, Eds. (Univ. of Arizona Press, Tucson, AZ, 2000), pp. 963–995.
15. S. Sahijpal, J. N. Goswami, A. M. Davis, L. Grossman, R. S. Lewis, *Nature* **391**, 559 (1998).
16. D. Weber, E. K. Zinner, A. Bischoff, *Geochim. Cosmochim. Acta* **59**, 803 (1995).
17. T. Z. LaTourrette, G. J. Wasserburg, *Earth Planet. Sci. Lett.* **158**, 91 (1998).
18. T. Z. LaTourrette, I. D. Hutcheon, *Lunar Planet. Sci.* **30**, 2003 (1999).
19. M. Gounelle et al., *Astrophys. J.* **548**, 1051 (2001).
20. K. D. McKeegan, M. Chaussidon, F. Robert, *Science* **289**, 1334 (2000).
21. M. Chaussidon, F. Robert, K. D. McKeegan, *Lunar Planet. Sci.* **33**, 1563 (2002).
22. K. K. Marhas, J. N. Goswami, A. M. Davis, *Meteorit. Planet. Sci.* **37** (suppl.), A94 (2002).
23. G. W. Lugmair, A. Shukolyukov, *Meteorit. Planet. Sci.* **36**, 1017 (2001).
24. L. E. Nyquist et al., *Lunar Planet. Sci.* **30**, 1604 (1999).
25. O. Bogdanovski, D. A. Papanastassiou, G. J. Wasserburg, *Lunar Planet. Sci.* **33**, 1802 (2002).
26. The $^{207}\text{Pb}/^{206}\text{Pb}$ isotopic chronometer is based on radioactive decay of two long-lived radionuclides: ^{235}U and ^{238}U (57). ^{235}U decays about six times faster than ^{238}U , and the $^{235}\text{U}/^{238}\text{U}$ atomic ratio decreases through geological time. Hence, the atomic ratio of stable radiogenic nuclides $^{207}\text{Pb}/^{206}\text{Pb}$, produced by decay of ^{235}U and ^{238}U , also changes with time. This ratio can be used to measure the time since formation of a U-bearing mineral or rock (e.g., chondrule or CAI). The $^{207}\text{Pb}/^{206}\text{Pb}$ chronometer has a number of unique features distinguishing it from other isotopic chronometers. Because the date calculation is based on isotopic composition of one element and does not include U/Pb ratio, it is free of analytical uncertainties in the U/Pb ratio. The $^{207}\text{Pb}/^{206}\text{Pb}$ date is also insensitive to recent fractionation of U and Pb in the nature or in laboratory (U/Pb fractionation still affects the determination of concordance of the U-Pb system, but not the Pb-Pb age). Exceptionally high precision of the Pb-Pb method is a consequence of high abundance of ^{235}U in the early solar system and its fast decay, which in combination caused fast accumulation of radiogenic ^{207}Pb . Relative errors $^{207}\text{Pb}/^{206}\text{Pb}$ dates in this age interval are about three times smaller than the relative errors in

the $^{207}\text{Pb}/^{206}\text{Pb}$ radiogenic isotope ratios from which the age is calculated. The precision of a date determined from highly radiogenic Pb isotopic ratios is mainly limited by the uncertainty in Pb isotopic fractionation in a mass-spectrometer. This uncertainty is typically between 0.03 and 0.1% (2σ) per mass unit, producing the uncertainty of 0.4 to 1.4 My in a single $^{207}\text{Pb}/^{206}\text{Pb}$ date.

27. C. Göpel, G. Manhés, C. J. Allègre, *Meteoritics* **26**, 338 (1991).
28. C. J. Allègre, G. Manhés, C. Göpel, *Geochim. Cosmochim. Acta* **59**, 1445 (1995).
29. Two varieties of Pb are present in rocks, including meteorites: common (or initial) Pb, which was incorporated into the mineral during its formation; and radiogenic Pb, which was accumulated by radioactive decay of U during the lifetime of the mineral. If the mineral contains U but no common Pb, the Pb present in it is a pure radiogenic component that can be directly used for age calculation. Unfortunately, U-bearing minerals free of common Pb are very rare in meteorites. If common Pb is present in a mineral along with radiogenic Pb, it has to be subtracted. Two approaches are used for Pb-Pb dating in the presence of common Pb: model date (more often called "model age") and isochron. In the model date approach, an isotopic composition of common Pb is assumed, and common Pb is subtracted from total Pb on the basis of the measured isotopic abundance of ^{204}Pb . In the isochron approach, a set of samples (mineral fractions, chondrules, or even whole meteorites) is assumed to be cogenetic, i.e., having the same age and the same initial common Pb. No particular common Pb composition is assumed, but the isochron model requires that the common Pb isotopic composition is homogeneous. In $^{207}\text{Pb}/^{206}\text{Pb}$ versus $^{204}\text{Pb}/^{206}\text{Pb}$ isochron plot, used in this study (Fig. 1), the y-axis intercept gives the radiogenic $^{207}\text{Pb}/^{206}\text{Pb}$ ratio and therefore the age, whereas the slope depends on the common Pb isotopic composition. The exact composition of common Pb cannot be determined from a Pb-Pb isochron, but can be estimated from the intercept of the isochron with a model Pb growth curve for the studied reservoir (57).
30. M. E. Zolensky, *Meteoritics* **26**, 414 (1991).
31. R. N. Clayton, T. K. Mayeda, *Geochim. Cosmochim. Acta* **63**, 2089 (1999).
32. M. K. Weisberg, M. Prinz, R. N. Clayton, T. K. Mayeda, *Geochim. Cosmochim. Acta* **57**, 1567 (1993).
33. A. N. Krot, A. Meibom, M. K. Weisberg, K. Keil, *Meteorit. Planet. Sci.*, in press.
34. A. N. Krot, K. Keil, *Meteorit. Planet. Sci.* **37**, 91 (2002).
35. A. N. Krot, J. Aléon, K. D. McKeegan, *Lunar Planet. Sci.* **33**, 1412 (2002).
36. K. K. Marhas, A. N. Krot, J. N. Goswami, *Meteorit. Planet. Sci.* **36**, A121 (2001).
37. A. N. Krot, M. K. Weisberg, M. I. Petaev, K. Keil, E. R. D. Scott, *Lunar Planet. Sci.* **31**, 1470 (2000).
38. A. N. Krot et al., *Meteorit. Planet. Sci.* **33**, 1065 (1998).
39. E. R. D. Scott, K. Keil, D. Stöeffler, *Geochim. Cosmochim. Acta* **56**, 4281 (1992).
40. A. N. Krot, A. A. Ulyanov, K. Keil, *Meteorit. Planet. Sci.* **35**, A93 (2000).
41. Mineral fractions were spiked with mixed ^{235}U - ^{205}Pb (or U-Th-Pb), ^{149}Sm - ^{150}Nd , and ^{85}Rb - ^{84}Sr tracer solutions. Mineral dissolution, chemical separations, isotopic analyses, and data reduction were performed as described (42, 43). Two procedure blanks were measured with each batch of samples. The Pb isotopic composition of the blank that was used for the correction is an average value ($\pm 2\sigma$) of 12 procedure blank determinations done previously and during the course of this study. Typical procedure blanks were 1×10^{-12} to 1.5×10^{-12} g for Pb, U, and Th. Because of small chondrule sizes, uncertainties in the blank corrections were a dominant source of the total errors. Isotopic fractionation and mass bias of the Daly detectors were determined with National Institute of Standards and Technology standards SRM-982 for Pb, U-500 for U, and an in-house Th isotope standard. Isochrons and weighted means, calculated with Isoplot-Ex version 2.49, are reported at 95% confidence level.